NANO LETTERS

2007
Vol. 7, No. 5
1240−1245

Magnetic Properties of Single-Crystalline CoSi Nanowires

Kwanyong Seo,[†,||] K. S. K. Varadwaj,[†,||] Paritosh Mohanty,[†] Sunghun Lee,[†] Younghun Jo,[‡] Myung-Hwa Jung,[‡] Jinhee Kim,[§] and Bongsoo Kim*[,†]

Department of Chemistry, KAIST, Daejeon 305-701, Korea, Quantum Material Research Team, KBSI, Daejeon 305-333, Korea, and Leading-Edge Technology Group, KRISS, Daejeon 305-600, Korea

Received January 16, 2007; Revised Manuscript Received March 22, 2007

ABSTRACT

We have observed unusual ferromagnetic properties in single-crystalline CoSi nanowire ensemble, in marked contrast to the diamagnetic CoSi in bulk. High-density freestanding CoSi nanowires with B20 crystal structure are synthesized by a vapor-transport-based method. The reaction of cobalt chloride precursor with a Si substrate produces high-aspect-ratio CoSi nanowires. The high-resolution transmission electron microscopy and electron diffraction studies reveal superlattice structure in CoSi nanowires with twice the lattice parameter of simple cubic CoSi lattice. The zero-field-cooled and field-cooled (ZFC-FC) measurements from the nanowire ensemble show freezing of the disordered surface spins at low temperatures. The magnetoresistance (MR) measurements of single nanowire devices show a negative MR whose magnitude gets larger at lower temperatures.

Transition metal monosilicides of Cr, Mn, Fe, and Co and solid solution alloys among them have a simple cubic B20 crystal structure and show a broad spectrum of magnetic and electrical transport properties.[1] While MnSi shows low-temperature helimagnetic order,[2] FeSi is a small-gap semiconductor with an anomalous temperature-dependent magnetic moment, and CoSi is a diamagnetic semimetal. Recent discovery of unusual positive magnetoresistance and a large anomalous Hall Effect in $Fe_{1-x}Co_xSi$ alloys showed possible use of metal silicides in the future Si-based spintronics technology.[3,4] In the search for ferromagnetic silicides carrying spin-polarized current, the epitaxially stabilized CoSi thin films on Si(111) has been considered as a potential candidate.[5] It has been among the major challenges in the field of nanotechnology to synthesize high-quality single-crystalline nanowires (NWs) that have the desired physical properties and to assemble and integrate these new materials into the device architecture.[6−9]

NWs often show distinct properties from their bulk counterparts because of radial confinement.[6,10] Because metal silicide NWs can be used as interconnects in integrated circuits and they are compatible with the processing of complementary metal-oxide-semiconductor (CMOS) devices,[11] synthesis of metal silicide NWs have been extensively studied recently. It has been demonstrated that the growth of self-assembled rare earth silicide NWs are induced by the anisotropic lattice mismatch between the NW and the silicon substrate.[12−15] There are also examples of synthesis of $CoSi_2$ and $FeSi_2$ NWs by endotaxial growth into the substrate.[16,17] Nevertheless, there have been continuing efforts to develop synthetic methods for free-standing silicide NWs to be used in bottom-up device applications. NiSi NWs are prepared by initial deposition of Ni on single-crystalline Si NWs followed by annealing and etching the extra metal.[11b,18] Syntheses of free-standing FeSi NWs by chemical vapor deposition were recently reported.[19,20] Jin and co-workers have synthesized CoSi NWs from single-source precursor by a MOCVD process and studied the electrical transport properties of the single NW devices.[21] Herein, we report the successful synthesis of free-standing single-crystalline CoSi NWs by a vapor transport method from anhydrous $CoCl_2$ precursor and measurement of the magnetic properties of the NW ensemble and magnetoresistance of a single CoSi NW.

Our synthetic approach is based on simple modification of the van Arkel method, used for the separation or purification of metals through vapor transport.[22] In this process, the exothermic reaction of metal and halogen is used to transport the metal from a mixture by halide formation. The metal is redeposited at a higher temperature by the reversible reaction. We have modified the process for the synthesis of silicide NWs: The metal halide precursor is evaporated and transported to the higher temperature zone by a carrier gas, where decomposition of metal halide and

* Corresponding author. E-mail: bongsoo@kaist.ac.kr.
[†] KAIST.
[‡] KBSI.
[§] KRISS.
[||] These authors contributed equally to this work.

10.1021/nl070113h CCC: $37.00
Published on Web 04/13/2007

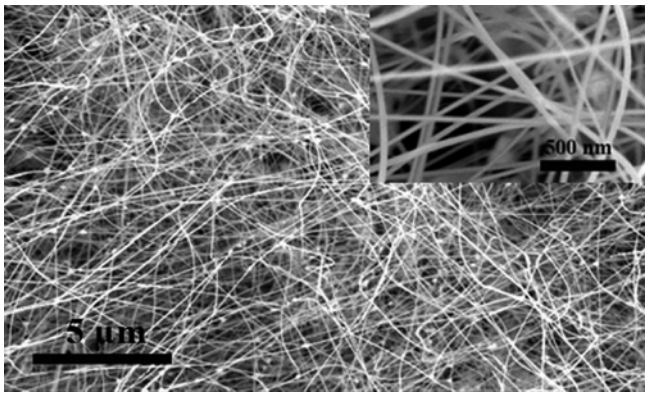

Figure 1. Representative SEM image of CoSi NWs. Inset shows high magnification SEM image of CoSi NWs.

reaction with the preheated silicon substrate occurs. In a typical synthesis, CoSi NWs were grown on Si(100) substrates with a native oxide layer. The substrates were placed in the middle of downstream zone in a conventional two-zone horizontal hot-wall furnace. Anhydrous $CoCl_2$ precursor was placed in an alumina boat in the middle of the upstream zone. The temperatures of both of the zones were independently controlled. After the quartz tube in the furnace was evacuated to less than 100 mTorr, 200 sccm Ar was purged into the system and pressure was adjusted to 500 Torr. The carrier Ar gas transported precursor vapor produced at 600 °C to the downstream zone maintained at 850 °C, where $CoCl_2$ decomposed and reacted with the Si substrate to form free-standing CoSi NWs.[23]

The morphology of the CoSi NWs was examined by field emission scanning electron microscopy (SEM) and transmission electron microscopy (TEM). The representative SEM image at low magnification in Figure 1 shows NWs in high density on the substrate. The high-magnification SEM image (inset in Figure 1) and TEM image (Figure 2a) clearly show the NWs with a clean and smooth surface. No secondary growth or extra structural features were observed. The NWs are tens of micrometers long and 20−60 nm in diameter.

To characterize the chemical composition and structure of the NWs, we carried out energy-dispersive X-ray spectrometry (EDS), high-resolution transmission electron microscopy (HRTEM), and electron diffraction (ED) studies. Figure 2a shows the TEM image and SAED pattern obtained from a representative CoSi NW. The diffraction pattern of the NW shows a regular spot pattern, which confirms the single-crystalline nature of the NWs. Less intense extra spots (indicated by the circle around the spot) are observed in the ED pattern at half the distance between the bright spots. The bright spots can be fully indexed to the cubic B20 type CoSi with a lattice constant 4.438 Å (space group *P*213, JCPDS card no. 72-1328).[23] The occurrence of weaker extra spots suggests the superlattice structure in the NW with twice the lattice constant of cubic CoSi. No change in the pattern or position of the extra spots could be seen when diffraction patterns are taken from different NWs. The ordered structure in the CoSi NWs may be induced by anisotropic growth of the NWs or due to periodic vacancy in some crystallographic sites.

Figure 2b shows the HRTEM image of a 20 nm diameter NW with clear lattice fringes and confirms again the single-

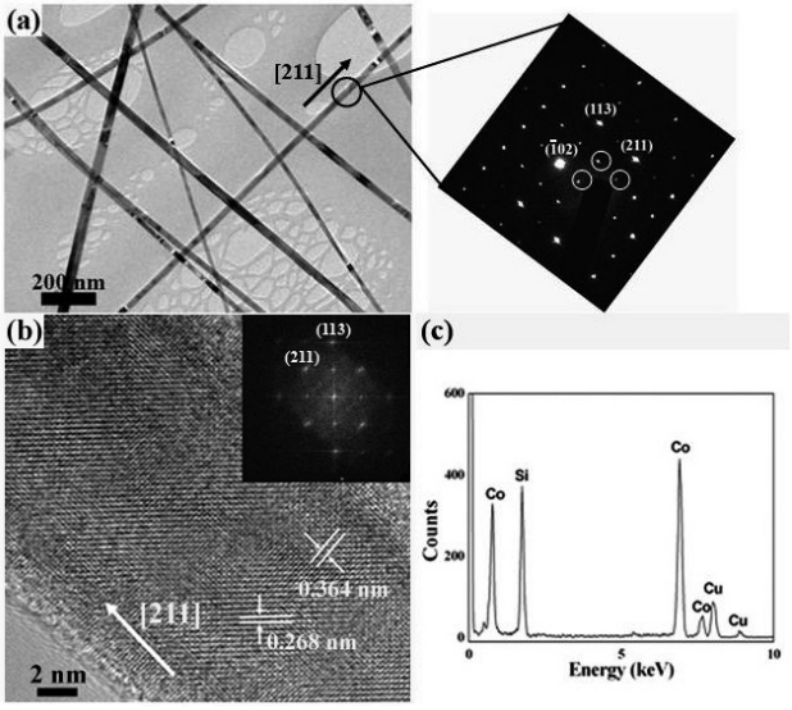

Figure 2. (a) Representative TEM image and SAED pattern. Black arrow in the TEM image shows the [211] growth direction. The SAED pattern is indexed for cubic CoSi NW down the [2$\bar{5}$1] zone axis, and white circles indicate supperlattice spots. (b) Representative high-resolution TEM image. The labeled distances of 0.268 and 0.364 nm correspond to the (311) and (211) superlattice planes, respectively, and the arrow shows the [211] growth direction. Inset in Figure 2b shows the two-dimensional fast Fourier transform (FFT). (c) Energy-dispersive X-ray spectrometry.

crystalline nature of the NW. The observed lattice planes with a spacing of 0.268 and 0.364 nm (shown in Figure 2b) are consistent with the (311) and (211) superlattice planes of the simple cubic CoSi, respectively. The two-dimensional fast Fourier transform (FFT) of the lattice-resolved image obtained from the HRTEM can also be indexed to a CoSi simple cubic lattice with a lattice constant of 4.438 Å. The growth of all the NWs are along [211] crystal planes, in contrast to the [110] growth direction of the CoSi NWs synthesized from an organometallic single-source precursor.[21] The EDS spectrum in Figure 2c from a single NW shows that Co and Si are the only elements present in the NWs (the peak for Cu is from the grid) in approximately a 1:1 atomic ratio.[23] The elemental line profiles show a uniform spatial distribution of Co and Si on the NW.[23]

The possible NW growth mechanism is derived from various experiments done in different reaction conditions. VLS growth is unlikely because no catalyst metal particles or thin films are employed in the synthesis. The SEM and TEM studies as shown in Figures 1 and 2a, respectively, also do not show the presence of any metal catalyst on the NW tip. Moreover, detailed EDS study from the tip and the stem of different NWs does not show significant deviation from approximately 1:1 composition of Co and Si. Large microparticles were produced when the temperature of the precursor heating zone was increased and/or pressure was decreased, whereas nanorods of shorter lengths were produced in the opposite case. The NW growth was found to be independent of the substrate orientation, as no change in the density or the structure of the synthesized CoSi NWs was observed on either the Si (111) or Si (100) substrates.

The $CoCl_2$ vapor reacts with a Si substrate at the high-temperature zone to form CoSi NWs by the following plausible reaction pathways.

$$2CoCl_2(g) + 3Si(s) \leftrightarrow 2CoSi(s) + SiCl_4(g)$$

$$CoCl_2(g) + SiCl_4(g) \leftrightarrow CoSi(s) + 3Cl_2(g)$$

These reactions show that CoSi phase can be formed either by the direct reaction of $CoCl_2$ with Si substrate or through a gas-phase reaction of $CoCl_2$ and $SiCl_4$. An optimum rate of the reactions, which is controlled by the precursor vapor pressure and the substrate temperature, facilitates the NW formation. In a further development of the reaction, we successfully changed the composition in NW and selectively synthesized free-standing Co_2Si NWs on a sapphire substrate placed on a Si base.[23]

The detailed magnetic properties of the as-grown CoSi NW ensemble on the Si substrate have been studied by using a superconducting quantum interference device (SQUID) magnetometer. In Figures 3 and 4, the measured magnetization is the sum of magnetic components from CoSi NWs and a Si substrate. The magnetic component from the Si substrate can be ignored because the magnetic moment of a Si substrate is lower than that of CoSi NWs by 2 orders of magnitude. The magnetization as a function of magnetic field was measured in the temperature range, $T = 2-380$ K

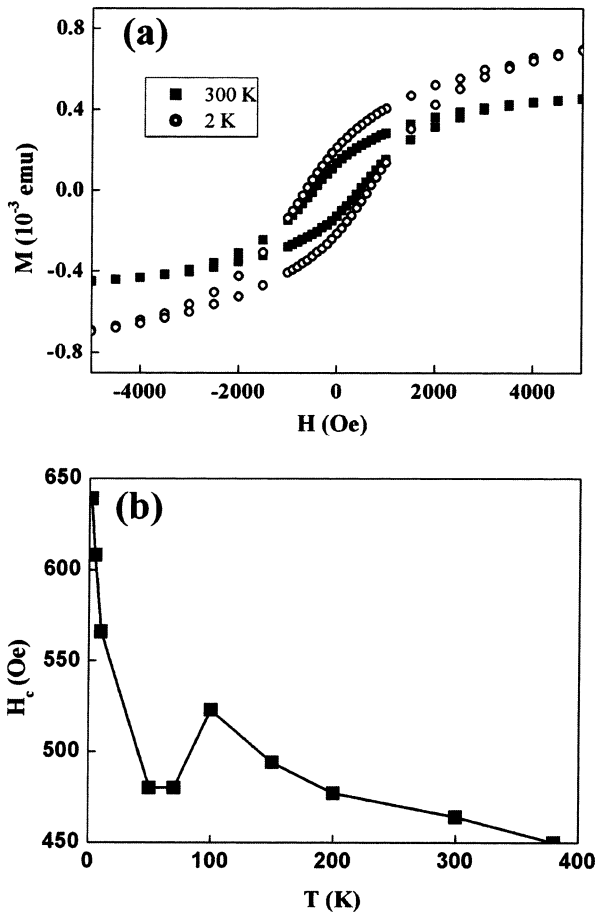

Figure 3. (a) Plot of M as function of H obtained from the NW ensemble at 2 and 300 K. (b) Plot of the coercive field (H_C) as a function of temperature obtained from the $M(H)$ curves.

(Figure 3a). The nonlinear room-temperature $M(H)$ curve with nonzero remnant magnetization and coercivity shows well pronounced ferromagnetic property of the NWs. Similar hysteresis loops are observed at lower temperatures down to 2 K, with gradual increase in the saturation magnetization. The magnetization, however, does not saturate at temperatures lower than 50 K, even when the applied magnetic field is increased to 10 kOe. The coercive field (H_C) obtained from the $M(H)$ curves is plotted as a function of temperature in Figure 3b. The H_C value does not change very much in the temperature range of 380 to 50 K, but increases steeply on further lowering of temperature.

It is rarely observed that diamagnetic materials become ferromagnetic in nanoforms. Nanoparticles of Au and Ag show ferromagnetism when capped by thiols.[24] The ferromagnetic properties in these materials are attributed to the change in electronic structure of the metal nanoparticles by the interaction with surface ligands. Ferromagnetism is also observed in various antiferromagnetic nanoparticles and NWs, and it is attributed to the uncompensated spins in two sublattices or reduced coordination of the surface spins.[25,26] The exchange bias between the surface spins and the antiferromagnetic core is known to produce a shift of the hysteresis loop for field-cooled and zero-field-cooled $M(H)$ measurements at the same temperature in these systems. CoSi itself is different from these materials in the sense that CoSi

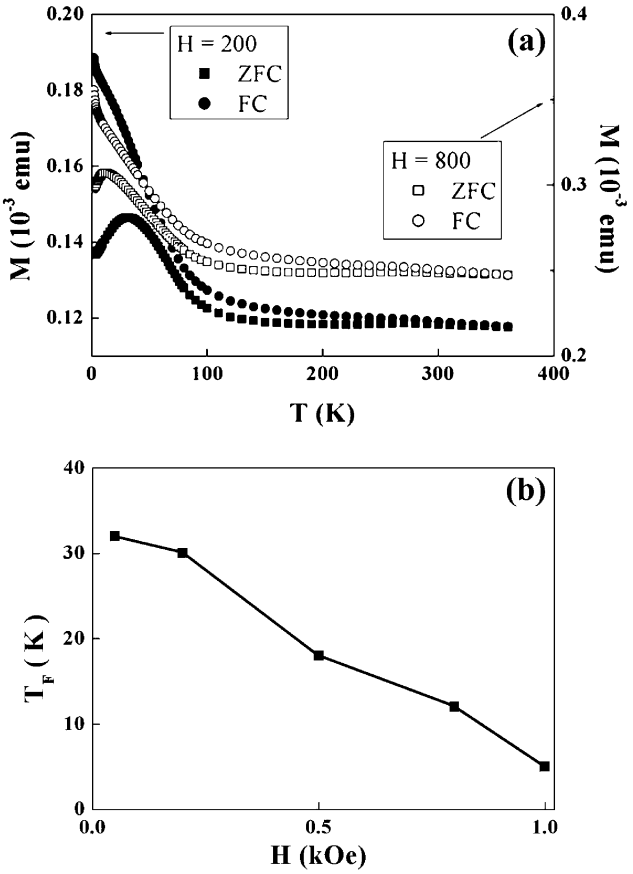

Figure 4. (a) Plot of *M* vs *T* obtained from CoSi NW ensemble at applied fields of 200 Oe (filled squares and circles) and 800 Oe (empty squares and circles). Squares and circles represent the ZFC and FC data, respectively. (b) Change in freezing temperature (T_F) with the applied magnetic field (*H*), obtained from the ZFC data.

is diamagnetic in the bulk despite half of the constituent atoms being ferromagnetic. In the light of the above discussion, the ferromagnetism observed in the CoSi NWs may be attributed to two possible origins. First, strain or structural defects in the crystal might induce ferromagnetism in the whole crystal. Second, the magnetic properties of the NW ensemble may be dominated by the reduced coordination of the surface Co atoms in the CoSi NWs, where surface-to-volume ratio is high. These surface spins not fully coordinated may act as a ferromagnetic surface layer on the NW.

We have recorded temperature-dependent zero-field-cooled (ZFC) and field-cooled (FC) magnetization measurements at various applied fields in order to gain further insight into the magnetic properties of CoSi NW ensemble. Figure 4a shows the temperature-dependent ZFC and FC magnetization measured under applied fields of 200 and 800 Oe, respectively. The ZFC curve shows a peak at 30 K under 200 Oe applied field, and the location of the peak shifts to lower temperatures under higher applied fields. At lower temperature, a distinctive divergence of FC and ZFC curves is observed with steep increase of FC magnetization, while the FC curves do not saturate up to 2 K. Complete convergence of FC and ZFC curves is not observed above the freezing temperature (T_F) up to room temperature. Such type of behavior is common with spin disorder systems (frustrated systems).[27] If spin disorder exists in the whole volume of a NW, reentrant spin-glass behavior is expected. But the results of frequency-dependent ac susceptibility and time relaxation measurements deny the possibility of reentrant spin-glass state in the NW core.[23] The reduced coordination of the surface spin, however, can contribute to the spin disorder observed in the FC and ZFC curves. These surface spins align themselves in the direction of the applied field at low temperatures. The enhanced coercivity below the freezing temperature as observed in the hysteresis loop (Figure 3) is also consistent with the freezing behavior observed in FC and ZFC curves (Figure 4). The freezing temperature gradually decreases at a higher applied field, and FC and ZFC curves completely merge with applied field higher than 1 kOe, when the anisotropy field of the surface spins is surpassed and the surface spins in the NWs are supposed to be saturated. Considering these results and taking into account the perfectly single-crystalline nature of the NWs, we could exclude the possibility of structural defects or strain being the origin of ferromagnetism, and we suggest that undercoordinated Co atoms on the surface of the NW covering a diamagnetic core induce the observed ferromagnetism in CoSi NWs.

The reaction of Co on a Si substrate has been thoroughly investigated by many groups. It has been shown that Co reacts with Si to form Co_2Si phase at 400 °C, subsequent annealing for longer time transforms Co_2Si into CoSi phase, and $CoSi_2$ phase is formed at about 600 °C.[28,29] In our synthesis of CoSi NWs, the reaction temperature is 850−900 °C. Therefore, the presence of any unreacted Co nanoparticles on the substrate is quite unlikely in this reaction condition. SEM, TEM, and EDS studies also showed only CoSi NWs on the substrate, and no other nanostructures were detected.

We further calculated the magnetic moment per surface Co atom from the saturation magnetization value of the 2 K *M*(*H*) curve. Simple calculations estimate that the percentage of surface Co atoms in the CoSi NWs is in the range of 1.47−4.34% after taking the distribution of NW diameters into consideration. We obtained an average magnetic moment of $1.37 \pm 0.53\ \mu_B$ per surface Co atom.[23] This value is in general agreement with the magnetic moment of Co^0 of 1.72 μ_B per Co atom.[30] This estimation provides substantial support for our hypothesis that surface Co atoms induce the observed ferromagnetism.

Transport studies and magnetoresistance (MR) measurements have been carried out on the individual CoSi NW. The device for the MR measurements was prepared by dispersing CoSi NWs on a SiO_2-coated Si substrate. The position of the NW was located in reference to the predefined marks and the nanoelectrodes of 20 nm Ti, and 80 nm Au were fabricated using standard electron-beam lithography technique. Figure 5a shows the SEM image of such a NW device. The electron transport measurements were carried out by a physical property measurement system (PPMS, Quantum design) using two-probe and four-probe configurations. The NW device shows linear current versus voltage

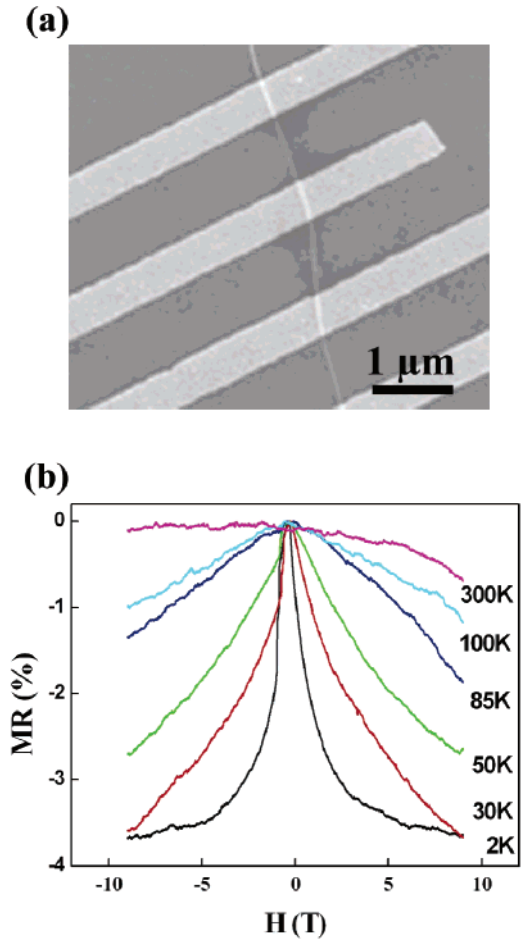

Figure 5. (a) SEM image of the NW device, (b) MR (%) of single CoSi NW at various temperatures.

curve, which confirms an ohmic contact between the NW and the electrodes. The resistivity measured at room temperature and 2 K is found to be 126.5 $\mu\Omega$ cm and 92.6 $\mu\Omega$ cm, respectively, which matches well with that reported for bulk single-crystalline CoSi (180 $\mu\Omega$ cm).[31] The MR measurements were done with the magnetic field applied parallel to the NW. The isothermal MR curves at 300, 100, 85, 50, 30, and 2 K are plotted in Figure 5b. The MR is defined as MR = $[R(H) - R(0)]/R(0)$, Where $R(H)$ and $R(0)$ are the resistances at an applied field (H) and zero field, respectively. MR of ~2.5% was seen at $T = 50$ K and $H = 9$ T, and MR becomes ~4% at $T = 2$ K and $H = 9$ T. The MR at 2 K shows saturation at the applied field higher than 4 T. Such negative MR can be explained by the reduction of scattering due to the alignment of spins by the applied magnetic field. These observations agree well with the freezing of disordered surface spins observed in the FC-ZFC curves from the NW ensemble.

In conclusion, we have synthesized high-density free-standing single-crystalline CoSi NWs. The synthesis process is a successful demonstration of controlled metal halide vapor transport by a modified van Arkel method and reaction of metal halide with silicon substrate to form silicide NWs. Moreover, this method may be further explored for the synthesis of transition metal silicide NWs with different silicon compositions. Structural characterization of the CoSi NWs by ED and HRTEM shows an ordered superlattice structure. Magnetic measurements of the CoSi NW ensemble show ferromagnetic property with low-temperature freezing of surface spins. The MR measurements on single NW devices show significant negative MR effect. The ensemble magnetic property is found to be in good agreement with the single NW MR. Ferromagnetic CoSi NWs may become one of the promising candidates for future spintronic applications.

Acknowledgment. This research was supported by a grant (code no. 06K1501-02620) from "Center for Nanostructured Materials Technology" under "21st Century Frontier R&D Programs" of the Ministry of Science and Technology, Korea. SEM and TEM analysis was performed at the Korea Basic Science Institute in Daejeon. We thank Prof. D. G. Churchill for helpful discussion.

Supporting Information Available: Experimental details; energy-dispersive X-ray spectrometry (EDS); analysis of SAED pattern for CoSi NWs; ac magnetic susceptibility and time relaxation data for CoSi NWs; synthesis of Co_2Si NWs on the sapphire substrate; calculation of magnetic moment. This material is available free of charge via the Internet at http://pubs.acs.org.

References

(1) Wernick, J. H.; Wertheim, G. K.; Sherwood, R. C. *Mater. Res. Bull.* **1972**, *7*, 1431.
(2) Pfleiderer, C.; Julian, S. R.; Lonzarich, G. G. *Nature* **2001**, *414*, 427.
(3) Manyala, N.; Sidis, Y.; DiTusa, J. F.; Aeppli, G.; Young, D. P.; Fisk, Z. *Nat. Mater.* **2004**, *3*, 255.
(4) Manyala, N.; Sidis, Y.; DiTusa, J. F.; Aeppli, G.; Young, D. P.; Fisk, Z. *Nature* **2000**, *404*, 581.
(5) Wu, H.; Kratzer, P.; Scheffler, M. *Phys. Rev. B* **2005**, *72*, 144425.
(6) Xia, Y.; Yang, P.; Sun, Y.; Wu, Y.; Mayers, B.; Gates, B.; Yin, Y.; Kim, F.; Yan, H. *Adv. Mater.* **2003**, *15*, 353.
(7) Lieber, C. M. *MRS Bull.* **2003**, *28*, 486.
(8) Cui, Y.; Zhong, Z.; Wang, D.; Wang, W. U.; Lieber, C. M. *Nano Lett.* **2003**, *3*, 149.
(9) Javey, A.; Guo, J.; Wang, Q.; Lundstrom, M.; Dai, H. *Nature* **2003**, *424*, 654.
(10) Jung, Y.; Lee, S.-H.; Ko, D.-K.; Agarwal, R. *J. Am. Chem. Soc.* **2006**, *128*, 14026.
(11) (a) Chueh, Y.-L.; Ko, M.-T.; Chou, L.-J.; Chen, L.-J.; Wu, C.-S.; Chen, C.-D. *Nano Lett.* **2006**, *6*, 1637. (b) Wu, Y.; Xiang, J.; Yang, C.; Lu, W.; Lieber, C. M. *Nature* **2004**, *430*, 61. (c) Zhang, S. L.; Ostling, M. *Crit. Rev. Solid State Mater. Sci.* **2003**, *28*, 1.
(12) Chen, Y.; Ohlberg, D. A. A.; Williams, R. S. *J. Appl. Phys.* **2002**, *91*, 3213.
(13) Nogami, J.; Liu, B. Z.; Katkov, M. V.; Ohbuchi, C.; Birge, N. O. *Phys. Rev. B* **2001**, *63*, 233305.
(14) Liu, B. Z.; Nogami, J. *J. Appl. Phys.* **2003**, *93*, 593.
(15) Preinesberger, C.; Becker, S. K.; Vandre, S.; Kalka, T.; Dahne, M. *J. Appl. Phys.* **2002**, *91*, 1695.
(16) He, Z.; Smith, D. J.; Bennet, P. A. *Phys. Rev. Lett.* **2004**, *93*, 256102.
(17) Liang, S.; Islam, R.; Smith, D. J.; Bennett, P. A.; O'Brien, J. R.; Taylor, B. *Appl. Phys. Lett.* **2006**, *88*, 113111.
(18) Decker, C. A.; Solanki, R.; Freeouf, J. L.; Carruthers, J. R.; Evans, E. R. *Appl. Phys. Lett.* **2004**, *84*, 1389.
(19) Schmitt, A. L.; Bierman, M. J.; Schmeisser, D.; Himpsel, F. J.; Jin, S. *Nano Lett.* **2006**, *6*, 1617.
(20) Ouyang, L.; Thrall, E. S.; Deshmukh, M. M.; Park, H. *Adv. Mater.* **2006**, *18*, 1437.
(21) Schmitt, A. L.; Zhu, L.; Schmeisser, D.; Himpsel, F. J.; Jin, S. *J. Phys. Chem. B* **2006**, *110*, 18142.

(22) van Arkel, A. E.; de Boer, J. H. *Z. Anorg. Allgem. Chem.* **1925**, *148*, 345.
(23) See Supporting Information.
(24) (a) Crespo, P.; Litrán, R.; Rojas, T. S.; Multigner, M.; de la Fuente, J. M.; Sánchez-López, J. C.; García, M. A.; Hernando, A.; Penadés, S.; Fernández, A. *Phys. Rev. Lett.* **2004**, *93*, 087204. (b) Lorenza, S.; Fiorani, D.; Scavia, G.; Imperatori, P.; Plunkett, W. R. *Chem. Mater.* **2007**, *19*, 1509.
(25) (a) Kodama, R. H.; Makhlouf, S. A.; Berkowitz, A. E. *Phys. Rev. Lett.* **1997**, *79*, 1393. (b) Wang, Y.; Yang, C. M.; Schmidt, W.; Spliethoff, B.; Bill, E.; Schüth, F. *Adv. Mater.* **2005**, *17*, 53. (c) Salabas, E. L.; Rumplecker, A.; Kleitz, F.; Radu, F.; Schüth, F. *Nano. Lett.* **2006**, *6*, 2977.
(26) Neel, L. In *Low Temperature Physics*; DeWitt, C., Dreyfus, B., de Gennes, P. D., Eds.; Gordon and Breach: New York, 1962; p 413.
(27) Dho, J.; Kim, W. S.; Hur, N. H. *Phys. Rev. Lett.* **2002**, *89*, 027202.
(28) Chattopadhyay, M. K.; Roy, S. B.; Chaudhary, S. *Phys. Rev. B* **2002**, *65*, 132409.
(29) Appelbaum, A.; Knoell, R. V.; Muraka, S. P. *J. Appl. Phys.* **1985**, *57*, 1880.
(30) Morris, A. H. *The Physical Principles of Magnetism*; IEEE: New York, 2001.
(31) Ren, W. L.; Li, C. C.; Zhang, L. T.; Ito, K.; Wu, J. S. *J. Alloys Compd.* **2005**, *392*, 50.

NL070113H